Magnetic properties across the YMnO3-BiFeO3 system designed for phase-change magnetoelectric response

M. Algueró, J.A. Quintana-Cilleruelo, O. Peña, A. Castro

Magnetic properties across the $YMnO_3$-$BiFeO_3$ system designed for phase-change magnetoelectric response

M. Algueró[a,*], J.A. Quintana-Cilleruelo[a], O. Peña[b] and A. Castro[a]

[a]Instituto de Ciencia de Materiales de Madrid (ICMM), CSIC. Cantoblanco, 28049 Madrid, Spain

[b]Sciences Chimiques de Rennes, UMR 6226, Université de Rennes 1. 35042 Rennes, France

*Corresponding author. E-mail address: malguero@icmm.csic.es (Miguel Algueró)

Abstract

Perovskite systems with structurally different multiferroic end members are being extensively investigated, because large phase-change magnetoelectric responses have been anticipated at the morphotropic phase boundaries (MPBs) between polymorphic forms with differentiated ferroic orderings. (1-x) $YMnO_3$-x $BiFeO_3$ is one such system, for which two continuous perovskite solid solutions with rhombohedral *R*3c and orthorhombic *Pnma* symmetries are present, and coexist across a wide compositional range. This might be a discontinuous MPB between a non-polar and a polar phase, at which the orthorhombic to rhombohedral transition may be electrically induced with a distinctive magnetic signature. In order to explore this possibility, magnetic properties have been characterized across the whole system, and relationships between perovskite crystal structure and magnetism have been established. Distinctive evolutions within each solid solution are revealed that define a region between x=0.6 and 0.9, where a non-polar orthorhombic ferromagnetic phase coexists with a polar rhombohedral antiferromagnetic one at room temperature.

Keywords: Single-Phase Multiferroic, Perovskite System, Morphotropic Phase Boundary, Magnetic Properties, Magnetoelectric Effects

1. Introduction

Magnetoelectric multiferroics are compounds that show coexistence of magnetic and electric ferroic orders [1,2]. They can present comparatively large magnetoelectric coefficients [2], and coupled electrical and magnetic domains [3]. A range of related magnetoelectric devices have been demonstrated or proposed, making use of the capability of controlling electric polarization with a magnetic field, and conversely of magnetization with an electric one [4]. It is especially interesting the possibility of switching ferromagnetic domains with the electric field, which would enable a new non-volatile random access memory that combine fast low-power electrical-writing and non-destructive magnetic-reading operations [5]. Other examples are electrically-tunable spintronics or microwave devices [6,7], to name but a few.

There are two general groups of multiferroics depending on whether the ferroic orders develop separately or not, usually referred to as type I and type II multiferroics [8]. Most work has concentrated on complex oxides, among which ABO_3 perovskite compounds stand out. This is the case of Bi-based perovskite oxides with site-by-site engineering for type I multiferroism. Rationale is placing Bi^{3+} with a stereochemically active electronic lone-pair at the A-site, which induces strong structural distortions and expectedly, yet not always, a ferroelectric polarization, and a magnetically active cation like Mn^{3+} or Fe^{3+} at the B-site [9]. Best example and one of the rare room temperature multiferroics is $BiFeO_3$ [10,11]. This is a ferroelectric perovskite oxide with rhombohedral *R*3*c* crystal structure [12], which also presents antiferromagnetic G-type spin ordering with a long-range incommensurate cycloidal modulation [13]. The ferroelectric transition takes place at ≈1103 K, while magnetic ordering develops within the polar rhombohedral phase at ≈643 K [11]. Spin canting and weak ferromagnetism appear if the cycloid is destroyed, which can be achieved by reducing

material system size below the characteristic length of the modulation (~62 nm) [14], by chemical modification [15] or imposing an in-plane strain [16]. Magnetic and ferroelectric domains are coupled [3], and electrically-driven deterministic reversal of the weak magnetization was recently accomplished in $BiFeO_3$ epitaxial films [17].

Type II or spin-driven multiferroics are magnetic ferroelectrics, for which the spontaneous polarization develops at a magnetic transition, usually involving rearrangements of complex antiferromagnetic orderings in the presence of competing spin interactions [18]. First reported compound was perovskite orthorhombic $TbMnO_3$, for which large magnetoelectric effects, basically changes and even reorientation of polarization under high magnetic field, have been described at low temperature [19]. This oxide is an example out of the series of $REMnO_3$ (RE: Rare Earth) manganese oxides with perovskite orthorhombic structure, which are thermodynamically stable for rare earth species with large ionic radius (from La down to Dy) [20]. A hexagonal phase is stable for RE with small radius (from Ho down to Lu), yet perovskite ones can still be obtained at high pressure [21]. This is also the case of $YMnO_3$, whose hexagonal phase is also multiferroic, but of type I [22-25].

The metastable perovskite orthorhombic phase with *Pnma* symmetry has been obtained by annealing at high pressure [21], mechanosynthesis in high energy planetary mills [26,27], or in thin form under high epitaxial strain [28]. Perovskite $YMnO_3$ shows an incommensurate antiferromagnetic order that develops at ~42 K. Improper ferroelectricity appears at a second magnetic transition at 28 K that has associated a distinctive dielectric anomaly [29,30].

Currently, an increasing activity is being concentrated on perovskite binary systems involving multiferroic end members. Attention initially focused on rhombohedral solid solutions based on $BiFeO_3$, aiming at either facilitating its preparation or improving properties, both electrical and magnetic [15]. Extensive work has been done on $BiFeO_3$-$REFeO_3$ systems, for which a structural

evolution from the rhombohedral *R*3*c* phase to an orthorhombic *Pnma* one has been described with RE substitution [31]. Large phase-change magnetoelectric responses have been anticipated, associated with an electrically induced phase transition between the *Pnma* and *R*3*c* polymorphic phases with differentiated magnetic orderings [32]. This might be a morphotropic phase boundary (MPB) between non-polar and polar phases, at which property enhancement by a polarization extension mechanism is expected [33]. Nonetheless, and alternatively, it could be the ferroelectric transition of $BiFeO_3$ that has been shifted below room temperature by RE substitution. Note that the high temperature paraelectric parent phase is also orthorhombic *Pnma* [11]. A MPB between non-polar and polar phases has been described for the $BiFeO_3$-$BiMnO_3$-$PbTiO_3$ ternary system [34].

Analogous non-polar orthorhombic *Pnma*-polar rhombohedral *R*3*c* MPBs can be expected in $REMnO_3$-$BiFeO_3$ binary systems, though this possibility has been poorly investigated, most probably due to difficulties in the synthesis and ceramic processing of the perovskite phases. An appealing system is (1-x) $YMnO_3$-x $BiFeO_3$ with multiferroic type II and type I end members. Indeed, a previous Rietveld study revealed the coexistence of orthorhombic *Pnma* and rhombohedral *R*3*c* polymorphs for perovskite phases with x between 0.8 and 0.9, and single rhombohedral phase for $x \geq 0.9$ [35]. Magnetic properties have been recently reported, but only for compositions between x=0.9 and 1 [36], Perovskite single-phase materials with x-values below 0.8 cannot be obtained by conventional solid state synthesis [37], which has prevented the complete characterization of the binary system.

Recently, we succeeded in obtaining perovskite phases all across the $YMnO_3$-$BiFeO_3$ system, free of secondary phases, by mechanosynthesis, and carried out structural characterizations that revealed the presence of two continuous perovskite solid solutions with orthorhombic *Pnma* and rhombohedral *R*3*c* symmetries, which coexisted in a broad compositional interval [27]. Here,

magnetic properties are presented and discussed as a function of x. Distinctive and differentiated evolutions across the two solid solutions are shown.

2. Materials and methods

Perovskite single-phase powdered samples of fourteen compositions across the whole (1-x) $YMnO_3$-x $BiFeO_3$ binary system, including x=0, 0.1, 0.2, 0.3, 0.4, 0.5, 0.6, 0.7, 0.8, 0.9, 0.925, 0.95, 0.975 and 1, were mechanosynthesized by high energy planetary milling of a stoichiometric mixture of precursor oxides in tungsten carbide media. Details of mechanical treatments, and the required parameters to attain the mechanosynthesis of the different perovskite compounds can be found elsewhere [27]. Phases were controlled by X-ray powder diffraction (XRD) with a Bruker AXS D8 Advance diffractometer. Patterns were collected between 12° and 60° (2θ), with 2θ increments of 0.05 and counting time of 0.2 s per step. The Cu-Kα doublet (λ = 1.5418 Å) was used in the experiments. Nanocrystalline perovskite phases were obtained for all compositions, which showed a distinctive evolution from a pseudo-orthorhombic symmetry to a pseudo-cubic one as x increased [27]. Sample morphology was monitored with a Philips XL 30 S-FEG scanning electron microscope, and submicron sized agglomerates of very small particles with size between 20 and 25 nm resulted.

Perovskite phases with enhanced crystallinity were obtained by thermal treatment of the as-mechanosynthesized samples. Phase stability under heating was an issue, and the maximum temperature perovskite phases withstood before decomposing varied with composition. Values are collected in Table 1, and ranged from 900 ºC and 825 ºC for x=0 and 0.925-0.975, respectively, down to 550 ºC for x=0.3-0.6. Not surprisingly, large differences in particle size resulted, which spanned from 65-80 nm for materials with x between 0.2 and 0.7, still in the nanoscale, up to 0.5-

0.7 μm for those with x between 0.9 and 1. Structural characterization by XRD sustained the presence of three regions with increasing x: (i) Orthorhombic phases between x=0 and 0.4, (ii) phase coexistence between orthorhombic and rhombohedral polymorphs between x=0.5 and 0.9, and (iii) rhombohedral phases for x > 0.9.

Polymorph fractions across the phase coexistence region were determined by a Rietveld approach, for which new XRD data with a reduced step size of 0.02º (2θ) and improved statistics were recorded between 20º and 90º (2θ). A mixture of orthorhombic *Pnma* and rhombohedral *R*3*c* phases was used as structural model, and phase percentages along with the respective lattice parameters of the two components were obtained as a function of x by Rietveld refinement of the patterns with the JANA2006 software [38].

Finally, magnetic properties of all thermally treated perovskite phases were characterized by SQUID magnetometry with a Quantum Design MPMS-XL5 apparatus. In a first step, magnetization *M* was measured after zero field cooling, during a subsequent heating and cooling cycle between 2 and 380 K under an applied field *H* of 100 Oe, which provided the zero field cooling (ZFC) and field cooling (FC) *M/H* ratio, or static susceptibility, as a function of temperature. Secondly, the low temperature isothermal, non-linear magnetization was measured under high magnetic fields up to 50 kOe.

3. Results

Examples of Rietveld refinements of the XRD data are given in Fig. 1. Results for x=0.3, 0.8 and 0.95 are shown that correspond to the orthorhombic *Pnma* single phase, phase coexistence, and

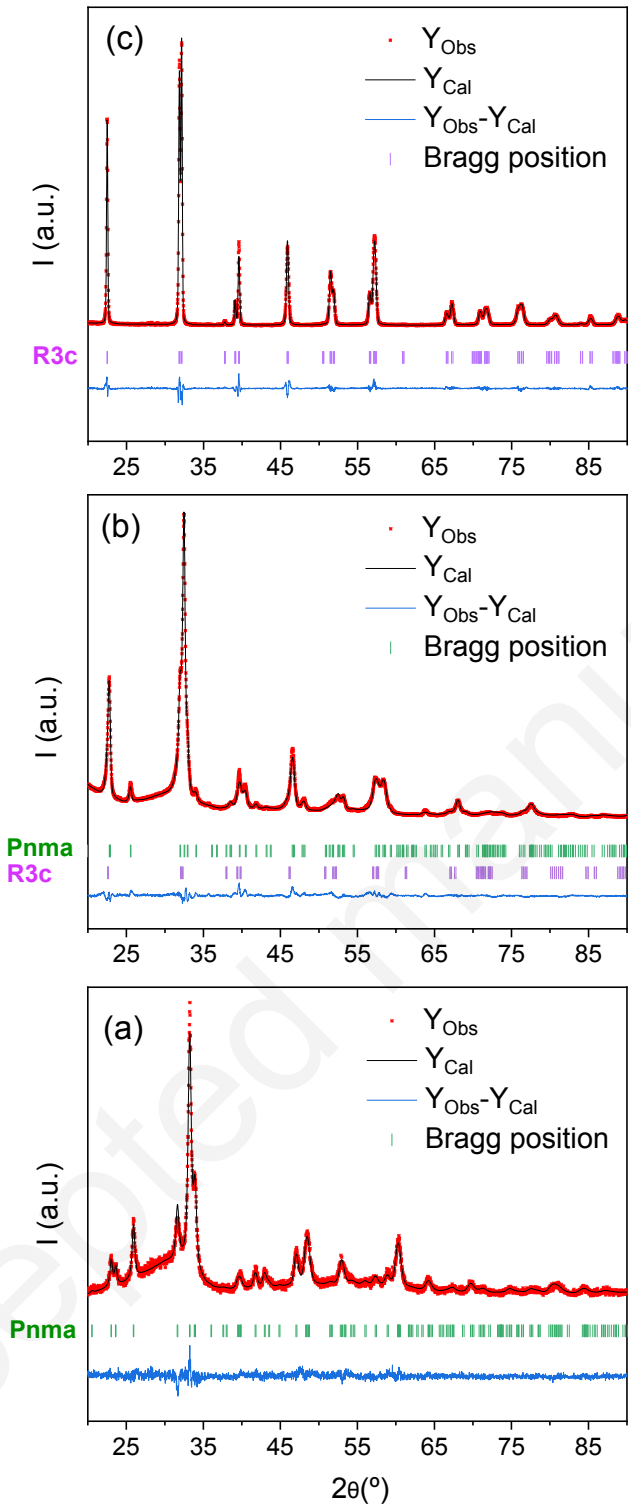

Fig. 1. Rietveld analysis of XRD data for the (1-x) $YMnO_3$-x $BiFeO_3$ materials with (a) x=0.3 assuming an orthorhombic *Pnma* structural model, (b) x=0.8 assuming a mixed orthorhombic *Pnma* and rhombohedral *R*3*c* model, and (c) x=0.95 assuming the rhombohedral *R*3*c* model. Refined orthorhombic fractions are provided in Table 1.

Table 1. Orthorhombic fraction (oF) and crystal lattice volume for the orthorhombic (Vo) and rhombohedral (Vr) polymorphic phases, as obtained from the Rietveld analysis of XRD data for the (1-x) $YMnO_3$-x $BiFeO_3$ materials. TT: Temperatures of the thermal treatments.

x	0	0.1	0.2	0.3	0.4	0.5	0.6
TT (ºC)	900	700	600	550	550	550	550
oF	1	-	-	1	-	0.925(6)	0.88(2)
Vo (Å^3)	225.53(9)	-	-	224.9(2)	-	229.26(4)	231.66(8)
Vr (Å^3)	-	-	-	-	-	348.9(4)	352.7(5)
x	0.7	0.8	0.9	0.925	0.95	0.975	1
TT (ºC)	600	700	750	825	825	825	750
oF	0.85(4)	0.77(4)	0.27(2)	-	0	-	-
Vo (Å^3)	234.2(2)	236.4(2)	240.4(3)	-	-	-	-
Vr (Å^3)	355.9(9)	365(2)	368.4(3)	-	371.0(2)	-	-

rhombohedral *R*3*c* single phase regions, respectively. Refinements for the remaining phase coexistence materials are provided in the supplementary information. As a summary, obtained polymorphic phase percentages and lattice cell volumes for the orthorhombic and rhombohedral components as a function of x are presented in Table 1.

Magnetic characterizations revealed distinctive relationships between the perovskite crystal structure and magnetism with differentiated properties for the orthorhombic and rhombohedral phases, and across the phase coexistence region. Magnetic properties are thus presented and preliminarily discussed separately for each of the three regions.

3.1. Orthorhombic phases ($0 \leq x \leq 0.4$)

Results on *M/H* ratio during ZFC/FC cycles are shown in Fig. 2(a) for the five orthorhombic phases. Regarding $YMnO_3$ (x=0), both ZFC and FC curves show the characteristic, sharp magnetic anomaly at $\approx$ 41 K associated with the antiferromagnetic ordering temperature T_N [26,29,39]. High field magnetization at 5 K was highly linear up 50 kOe with no hysteresis, as shown in Fig. 2(b).

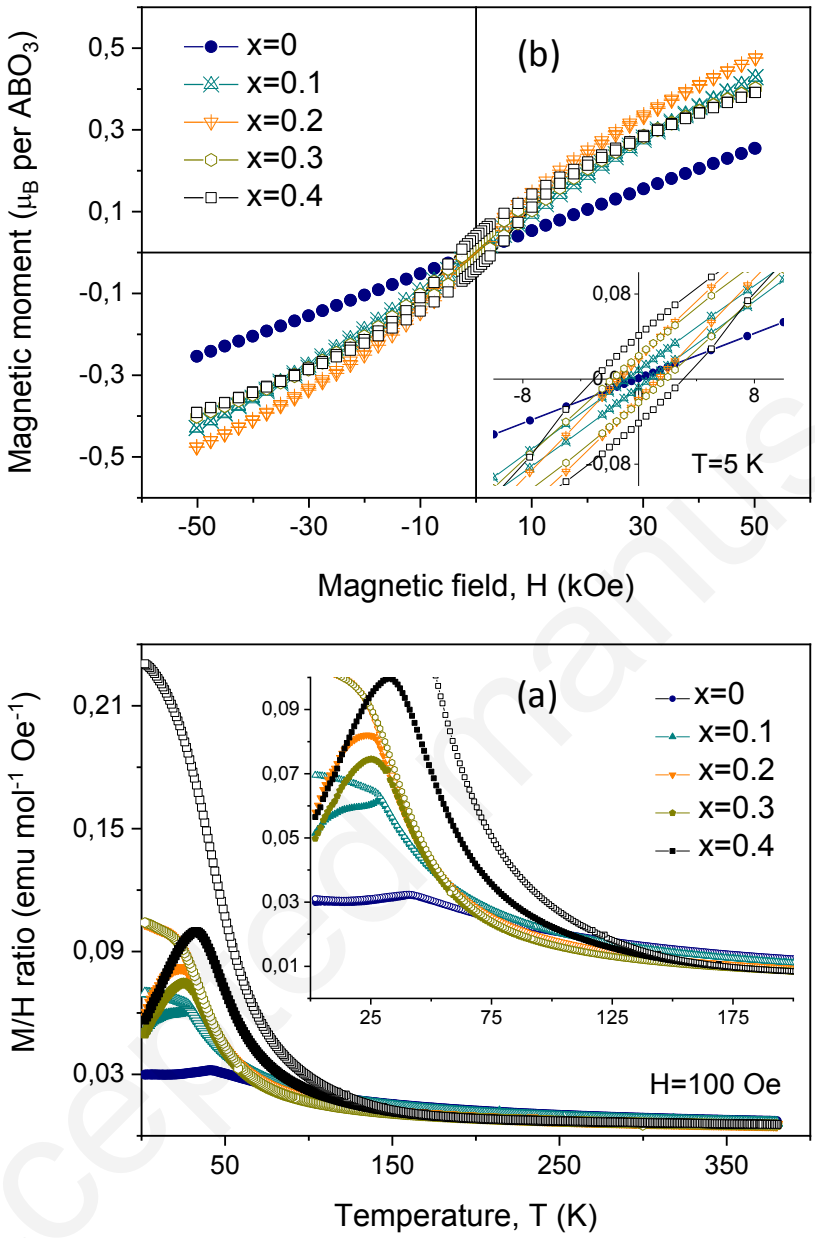

Fig. 2. (a) Temperature dependence of the ZFC (close symbols) and FC (open symbols) static susceptibility, and (b) isothermal magnetization at 5 K for orthorhombic single-phase (1-x) $YMnO_3$-x $BiFeO_3$ materials.

The ZFC curve for x=0.1 also shows a similarly sharp magnetic anomaly, but at ≈ 28 K. This suggests the shift of the Neel temperature towards low temperature after the substitution of Bi^{3+}/Fe^{3+} for Y^{3+}/Mn^{3+} in the perovskite. Besides, significant irreversibility develops below this temperature, so that the FC curve does not present the maximum in *M/H*, but this ratio keeps increasing on further cooling down to 2 K. Irreversible behaviour is usually associated with the occurrence of spin canting and weak ferromagnetism, which is also indicated by the appearance of hysteresis in the high field magnetization (see inset in Fig. 2(b)).

Maxima in ZFC curves are also found for x=0.2, 0.3 and 0.4, yet broadened. Their positions show a distinctive evolution with x, so that it is further shifted down to 23 K for x=0.2, yet the trend is reversed above this x-value and orthorhombic phases with x=0.3 and 0.4 present the *M/H* maxima at 26 and 33 K, respectively.

Irreversibility is also found for phases with x >0.1 with increasing values of *M/H* ratio after field cooling. Indeed, the FC magnetization increases from ≈0.0695 emu mol^{-1} Oe^{-1} for x=0.1 up to 0.104 emu mol^{-1} Oe^{-1} for x=0.2 at 2 K, it seems to saturate for x=0.3, but steeply increases again up to 0.231 emu mol^{-1} Oe^{-1} for x=0.4. It is remarkable that irreversibility for these phases (x=0.2, 0.3 and 0.4) start above the maxima in ZFC, and that temperature at which ZFC and FC curves split clearly increases with x (see inset in Fig. 2(a)), so that it is ~65, 90 and 160 K for x=0.2, 0.3 and 0.4, respectively.

An increasing canting and ferromagnetic component with x can be thus assumed in this first region. This is confirmed by the hysteresis of the high field response at 5 K, shown in Fig. 2(b). Both remnant magnetization M_r and coercive field H_c steadily increase with x up to values of 0.041μ_B per ABO_3 unit and 3.1 kOe, respectively, for x=0.4. Note that surfaces can also introduce weak ferromagnetism in antiferromagnetic nanoparticles, associated with uncompensated spins at the boundaries [14]. However, and even if nanostructured, particle size remains between 65 and

80 nm in these phases and hardly changes with composition between x=0.2 and 0.4 (and actually up to 0.7) Therefore, the described evolution is not a surface effect, but a true bulk one. Determination of ordering temperatures for these phases is not straightforward, because irreversibility starts well above the temperatures at which maxima in the derivative of the FC curves occur. These maxima are commonly taken as the Curie temperature of a ferromagnet, and they take place at 32, 34 and 40 K for x=0.2, 0.3 and 0.4, though irreversibility has started well above the respective maxima. Temperatures at which irreversibility sets out are usually taken as ordering ones when this occurs.

3.2. Phase coexistence ($0.5 \leq x \leq 0.9$)

Results on the *M/H* ratio during ZFC/FC cycles are shown in Fig. 3(a) and 4(a) for the five compositions placed at the phase coexistence region, which showed decreasing fractions of orthorhombic phase as x increased. Corresponding high field magnetizations are given in Fig. 3(b) and 4(b) at 5 K.

ZFC/FC curves for x=0.5 and 0.6 with orthorhombic phase fractions of 0.925 and 0.88, respectively, are given in Fig. 3(a). *M/H* evolution during the ZFC/FC cycle for x=0.5 is qualitatively analogous to that of x=0.4, also included for comparison. The ZFC curve shows the broad maximum, further shifted up to 47 K. The temperature at which irreversibility starts is also shifted towards high temperature, so that ZFC and FC curves split at ~215 K for x=0.5. FC magnetization at 2 K is highly enhanced up to a value of ≈0.877 emu mol^{-1} Oe^{-1}. Hysteresis in the high field response at 5 K is similarly increased with M_r and H_c values of 0.066μ_B per ABO_3 unit and 4.0 kOe, respectively (see Fig. 3(b)).

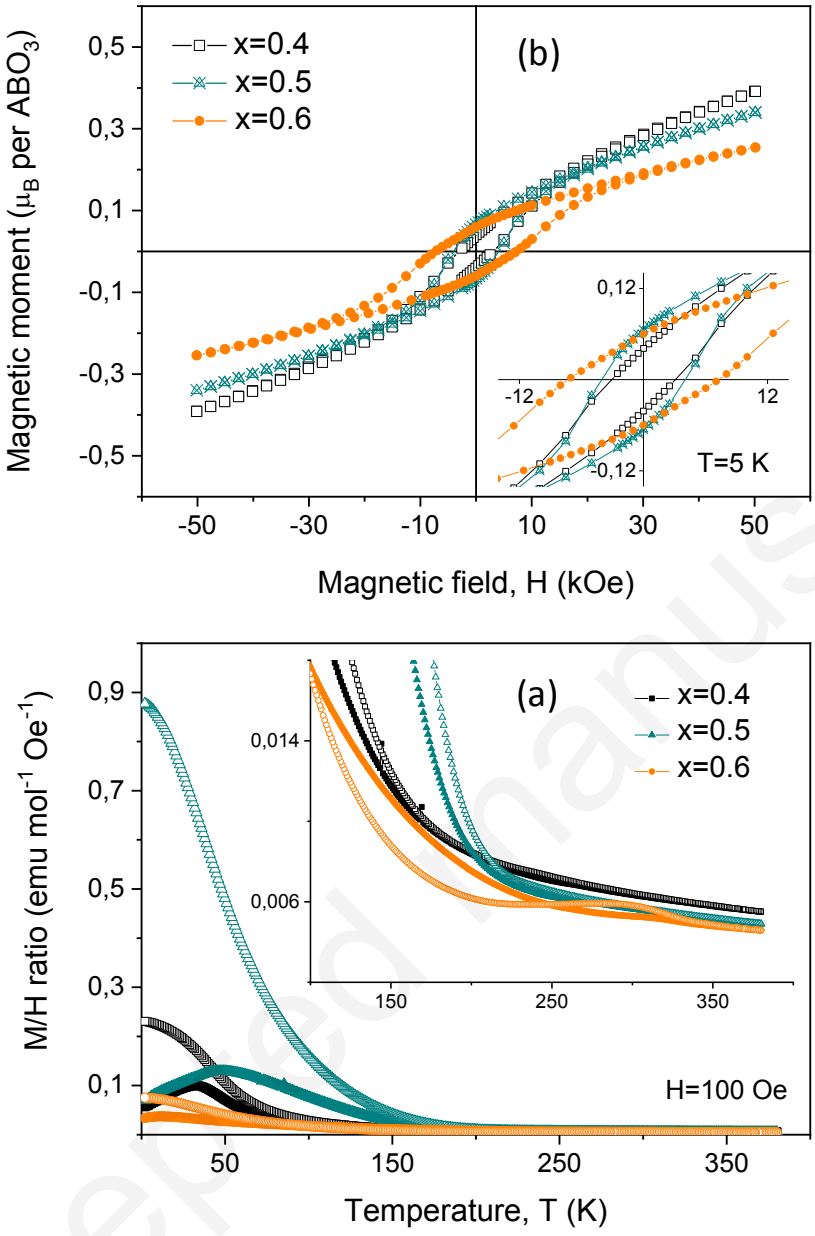

Fig. 3. (a) Temperature dependence of the ZFC (close symbols) and FC (open symbols) static susceptibility, and (b) isothermal magnetization at 5 K for (1-x) $YMnO_3$-x $BiFeO_3$ materials with x=0.5 and 0.6 in the phase coexistence region. Results for the orthorhombic phase with x=0.4 are included again to facilitate comparison with the previous figure.

Roughly, all orthorhombic phases between x=0.2 and 0.5, either single-phase or the majority polymorphic form, present a consistent evolution with x at constant particle size, so that they show a maximum in the ZFC curve at an increasing temperature. Irreversibility is progressively enhanced, and starts at a temperature that also increases with x, with growing FC magnetization at 2 K. This suggests canted antiferromagnetism with increasing ferromagnetic component, confirmed by the hysteresis in the high field magnetization at 5 K.

The magnetic behavior is modified from x=0.6, even if x=0.6, 0.7 and 0.8 still have orthorhombic phase fractions above 0.75. Although maxima in ZFC are found for x=0.6 and 0.7, they take place at strongly reduced temperatures of 8 and 5 K, respectively, while no maximum is found for x=0.8. This suggests the disappearance of the antiferromagnetic ordering. There is still irreversibility and thus, ferromagnetism that starts at ~335 K for x=0.6, and above the measuring range for x=0.7 and 0.8. However, FC magnetization at 2 K highly decreases above x=0.5, so that it is only ≈0.075 emu mol^{-1} Oe^{-1} for x=0.6. Besides, the FC curve on cooling crosses the ZFC, so that the FC *M/H* ratio is below the ZFC one in a certain range of temperatures.

This behavior is also found for x=0.7 and 0.8 over different temperatures ranges, and suggests the presence of a ferromagnetic phase that becomes magnetized during ZFC, and maintains the magnetization during subsequent FC (the ordering temperature is above the measuring range). This might be an impurity below the sensitivity of the XRD technique, but also the orthorhombic phase itself that is ferromagnetic for x ≥ 0.6. Recall that irreversibility starts at ~335 K for x=0.6 and above the measuring range for x=0.7 and 0.8. Consistently, the high field magnetization at 5 K still shows significant hysteresis with M_r values of 0.060 and 0.036μ_B per ABO_3 unit, and with H_c values of 7.3 and 8.4 kOe for x=0.6 and 0.7, respectively. However, no hysteresis is found for x=0.8 (see Fig. 4(b)).

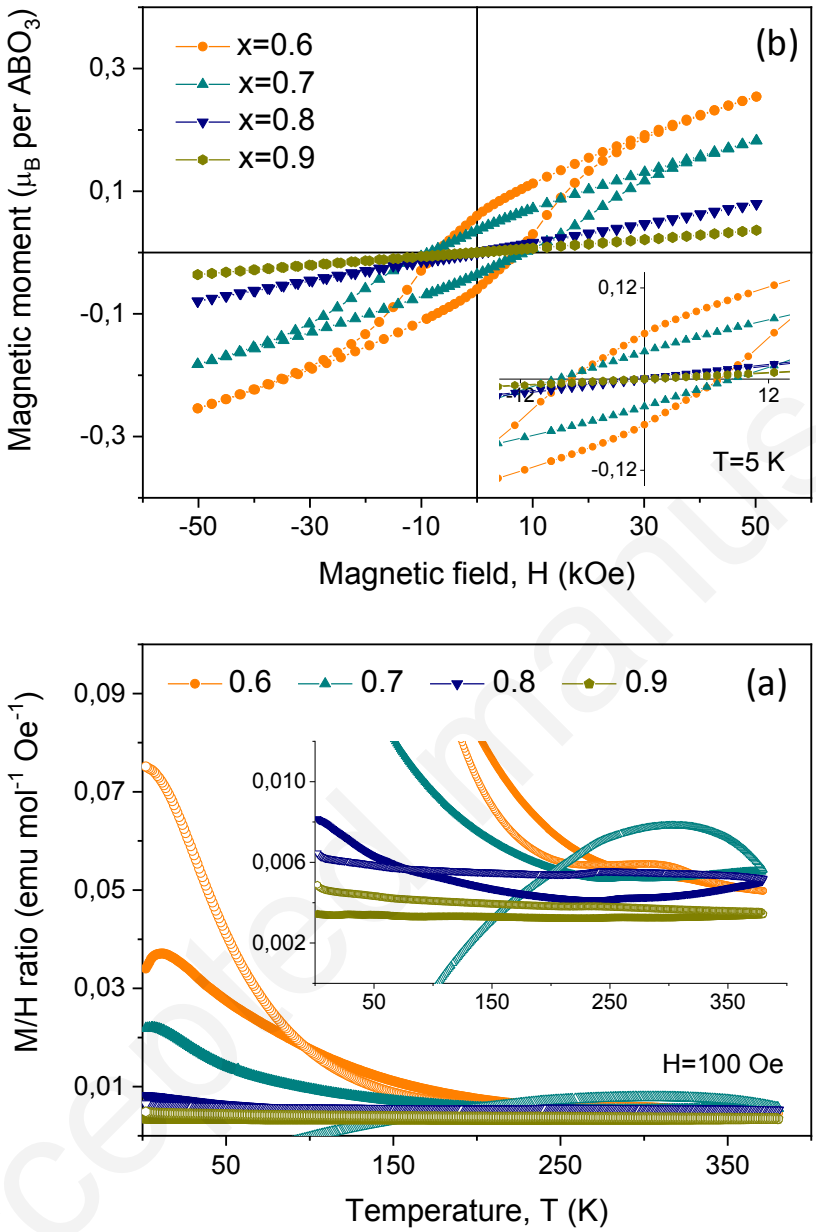

Fig. 4. (a) Temperature dependence of the ZFC (close symbols) and FC (open symbols) static susceptibility, and (b) isothermal magnetization at 5 K for (1-x) $YMnO_3$-x $BiFeO_3$ materials with x=0.7, 0.8 and 0.9 in the phase coexistence region. Results for the material with x=0.6 are included again to facilitate comparison with the previous figure.

x=0.9 is the first composition with orthorhombic fraction below 0.5 and thus properties are expected to be dominated by the rhombohedral phase. Indeed, its magnetic response is very different. The ZFC curve shows a small magnetization that gradually increases with temperature up to the maximum temperature reached. On the contrary, FC curve shows a distinctive increase of *M/H* ratio on cooling, so that an increasing irreversibility develops. High field magnetization at 5 K is hysteresis free and highly linear, but for a slight upturn at very high fields. We will discuss this overall behavior in the next section when addressing rhombohedral phases, but it strongly suggests antiferromagnetism with an ordering temperature above the measuring range.

3.3. Rhombohedral phases (0.925 ≤ x ≤ 1)

Results on *M/H* ratio during ZFC/FC cycles are shown in Fig. 5(a) for the four rhombohedral phases. Similarly to x=0.9 with rhombohedral fraction of 0.73, all ZFC curves show the gradual increase of magnetization with temperature up to 380 K, suggesting the presence of antiferromagnetic ordering with a Neel temperature above the measuring range [40]. This is certainly the case for $BiFeO_3$ (x=1), which presents G-type antiferromagnetic spin arrangement with a long-range incommensurate cycloidal modulation that emerges at 643 K [11]. Differential thermal analysis (DTA) shows a characteristic reversible thermal effect associated with the antiferromagnetic transition, and analogous thermal effects have been reported for x=0.9, 0.925 and 0.95 at 499, 573 and 616 K, respectively [27]. Transition would then shift towards high temperature with increasing x, and it is already above the current measuring range for x=0.9.

All rhombohedral phases are thus antiferromagnetic. Main compositional effect is magnetization values that are significantly higher for x=0.925 and 0.95 at 380 K: 0.063 and 0.0102 emu mol^{-1} Oe^{-1}, respectively, than for x=0.975 (0.0031 emu mol^{-1} Oe^{-1}) and x=1 (0.0025 emu mol^{-1} Oe^{-1}). A value of 0.0034 emu mol^{-1} Oe^{-1} was found for x=0.9.

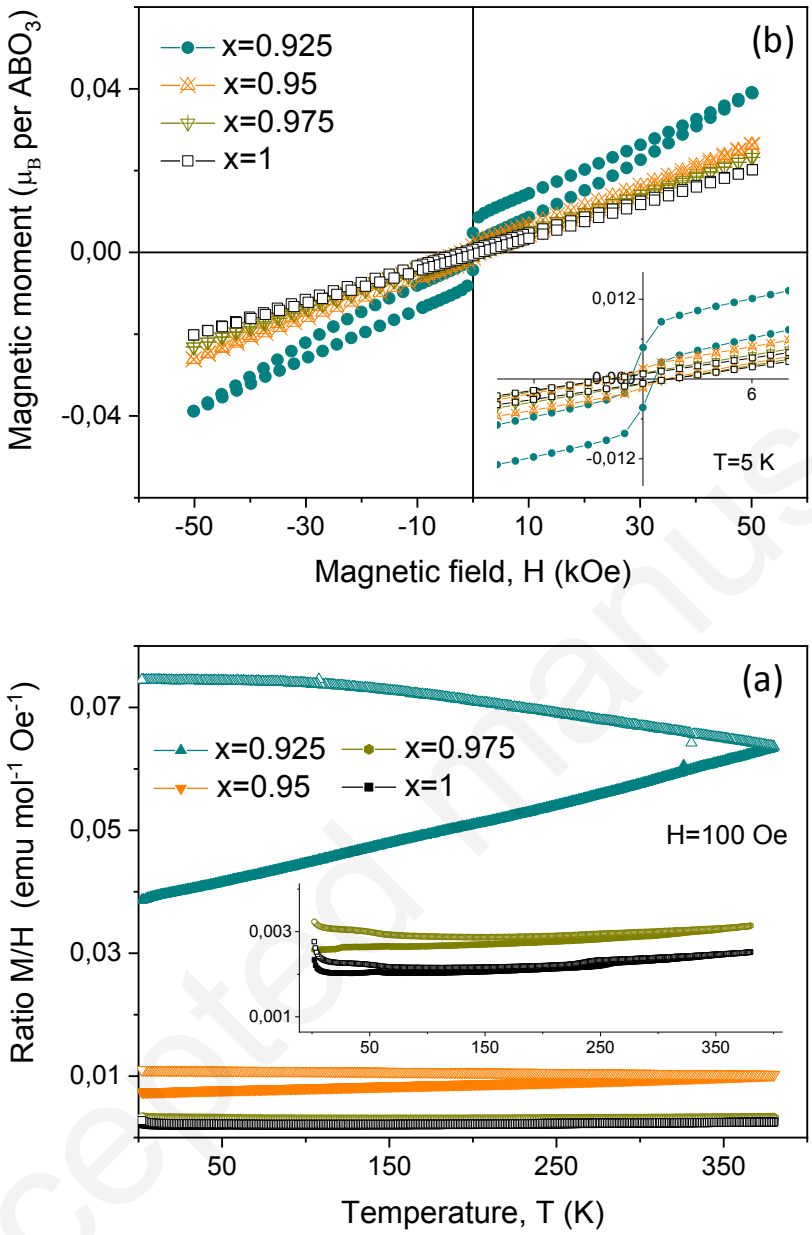

Fig. 5. (a) Temperature dependence of the ZFC (close symbols) and FC (open symbols) static susceptibility, and (b) isothermal magnetization at 5 K for rhombohedral single-phase (1-x) $YMnO_3$-x $BiFeO_3$ materials.

Irreversibility is present for all composition, yet it starts at 380 K for x=0.925 and 0.95, and at lower temperatures for x=0.975 and 1. Much higher FC magnetizations were found for x=0.925 and 0.95 at 2 K: 0.074 and 0.011 emu mol^{-1} Oe^{-1}, than for x=0.975 (0.0032 emu mol^{-1} Oe^{-1}) and x=1 (0.0028 emu mol^{-1} Oe^{-1}). Irreversibility for $BiFeO_3$ single crystals has been related to low temperature spin-glass behavior, which also results in weak ferromagnetism below the freezing temperature [41]. Indeed, note in Fig. 5(b) the non-negligible hysteresis in the high field response of x=0.975 and 1 at 5 K.

Irreversibility for x=0.925 and 0.95 most probably has a different origin, for it already starts at the beginning of the FC curve at 380 K, and significantly higher FC magnetizations develop. Spin canting appears in $BiFeO_3$ when the cycloid modulation is destroyed, an effect that can be induced by chemical substitutions like in $Bi_{1-x}A_xFeO_3$ with A=Ca, Sr, Ba and Pb [15]. Similar effects have been described for the $BiFeO_3$-$BiMnO_3$-$PbTiO_3$ ternary [42], and could also happen in $YMnO_3$-$BiFeO_3$. Note that the enhanced irreversibility for x=0.925 and 0.95 is accompanied by the appearance of a new, distinctive ferromagnetic contribution that adds to that of the frozen spin-glass at 2 K.

4. Discussion

Coexistence of two continuous perovskite solid solutions with orthorhombic and rhombohedral symmetry takes place over a wide range of compositions in the $YMnO_3$-$BiFeO_3$ binary system. This might indicate the presence of a non-polar/polar morphotropic phase boundary in the system, yet of a different nature to that of MPBs between polar rhombohedral and tetragonal phases described in the perovskite $Pb(Zr,Ti)O_3$, $BiScO_3$-$PbTiO_3$ or $Bi_{1/2}Na_{1/2}TiO_3$-$BaTiO_3$ systems, and characterized by converging lattice distortions on approaching the boundary, presence of intermediate bridging

phases and narrow compositional coexistence regions [43-45]. Similarly-wide phase coexistence has been anticipated by a first principles study of $BiFeO_3$-$BiCoO_3$, associated with two stable continuous solid solutions of rhombohedral and tetragonal symmetries with very close energies [46]. This case was referred to as "discontinuous" as compared with conventional "continuous" MPBs because lattice distortions diverge on approaching the boundary. The same theoretical investigation predicted large phase-change magnetoelectric responses, associated with an electrically induced phase transition between the *P*4*mm* and *R*3*c* polymorphic phases with differentiated magnetic orderings [46].

Large phase-change magnetoelectric responses have also been anticipated for $BiFeO_3$-$REFeO_3$ systems, associated in this case with an electrically induced phase transition between non-polar *Pnma* and polar *R*3*c* phases [32]. Analogous effects might be obtained in the $YMnO_3$-$BiFeO_3$ system if the two polymorphs had different magnetic orderings. Indeed, magnetic characterizations have revealed distinctive and differentiated magnetic properties for the two polymorphic forms, which also evolve within each solid solution.

Orthorhombic phases are present in (1-x) $YMnO_3$-x $BiFeO_3$ from x=0 up to x=0.9, as single phase up to x=0.4 and as majority polymorphic form from x=0.5 up to x=0.8. Magnetic critical temperatures: that is, positions of the maximum *M/H* ratio in ZFC (T_M^{ZFC}), of the maximum derivative in FC ($T_M^{dFC/dT}$), and of the onset of irreversibility (T_{Irrev}), are given in Fig 6(a) as a function of x. Three compositional intervals can be distinguished across the orthorhombic solid solution regarding its magnetic response, and specifically the evolution of T_M^{ZFC}. Note that x=0.9 has an orthorhombic fraction of only 0.27 and thus, its magnetic response is dominated by the majority rhombohedral phase, as indicated by T_M^{ZFC} being the maximum temperature attained during measurements. First interval would comprise x=0 and 0.1 that show both close T_M^{ZFC}, $T_M^{dFC/dT}$ and T_{Irrev} values that decrease with the substitution of Bi^{3+}/Fe^{3+} for Y^{3+}/Mn^{3+}. Basically, this indicates a reduction of the Neel temperature. The specific nature of the AFM ordering of $YMnO_3$ (x=0) is

controversial [30]. It has been described as a collinear incommensurate, sinusoidal spin arrangement related to E-type antiferromagnetism (this configuration is obtained in the commensurate case, i.e. when the spin sine wave vector *q* takes a value of 0.5) [39]. However, improper ferroelectricity exists, which is not compatible with the incommensurate sine wave. Alternatively, an also incommensurate, but non-collinear spiral configuration, analogous to that of $TbMnO_3$ has been proposed [28]. This is compatible with ferroelectricity and indeed, an electrical study of epitaxial films has shown polarization direction, and its rotation under magnetic fields to be consistent with this arrangement [28].

The decrease of the Neel temperature could be anticipated from the reduction in the number of Mn^{3+}-O^{2-}-Mn^{3+} bonds and thus, of antiferromagnetic superexchange interactions. Besides, irreversibility develops as a result of the substitution, which suggests the appearance of spin canting and of a weak ferromagnetic contribution. Difference between FC and ZFC curves at 2 K is given in Fig. 6(b) as a measurement of this irreversibility. The breaking ferromagnetic component is most probably associated with the new double exchange Mn^{3+}-O^{2-}-Fe^{3+} interactions. However, a pure structural effect cannot be disregarded, for both substitutions are expected to have significant effects in the perovskite distortion and thus, in bonding angles. Previous structural characterization showed a decrease of the orthorhombic cell volume from x=0 up to 0.2 [27]. Note that the latter composition can be seen as a transition one between this interval and the next one. Volume shrinkage was associated with the decrease of the Jahn-Teller distortion as a result of the reducing number of Mn^{3+}-O^{2-}-Mn^{3+} bonds. This offsets the expansion anticipated from the large ionic radius of Bi^{3+} (1.17 Å) as compared with Y^{3+} (1.019 Å).

Second interval would cover compositions x=0.3, 0.4 and 0.5. All T_M^{ZFC}, $T_M^{dFC/dT}$ and T_{Irrev} increase with x, as well as the difference between $T_M^{dFC/dT}$ and T_{Irrev} (see Fig. 6(a)). As already said, x=0.2 would be then an intermediate or transition composition between two magnetic regimes: T_M^{ZFC} decreases in relation to x=0.1, but $T_M^{dFC/dT}$ does not change and T_{Irrev} increases. Remarkably,

irreversibility is boosted above x=0.3. (see Fig. 6(b)). Note that x=0.5 is the composition, for which the number of Mn^{3+}-O^{2-}-Fe^{3} bonds and thus, of ferromagnetic interactions is maximized. High field response at 5 K also reflects the change of behaviour, and the magnetization at 50 kOe that continuously increased up to x=0.2, decreases above this x-value (see Fig. 6(b)). Structurally, x=0.3 is the composition at which the tendency of the orthorhombic cell volume with x changes, so that it continuously increases from x=0.3 up to x=0.9 (see ref. 27 and results of the Rietveld refinements in Table I). An evolution from E-type to A-type AFM ordering has been described for orthorhombic $REMnO_3$ perovskites as the ionic radius of the rare earth increases, as a result of increasing superexchange Mn-O-Mn bonding angles. Non-collinear spiral configurations appear in the intermediate ionic radius range as a result of competing interactions. Actually, $YMnO_3$ is thought to be at the boundary between E-type and spiral configurations [28], and could present one or another AFM ordering depending on boundary conditions (for instance an in-plane strain field in films) or the concentration of point defects (basically Mn^{4+}). The change of behavior observed at x=0.2 might then reflect an evolution from E-type to a spiral configuration. This hypothesis, however, would require neutron diffraction studies on highly crystalline samples, not currently available, to be demonstrated.

Third interval would comprise compositions with x=0.6, 0.7 and 0.8 (and probably 0.9 though the magnetic response of the minority orthorhombic phase cannot be isolated). A distinctive drop of T_M^{ZFC} is observed in this region down to 8 and 5 K, for x=0.6 and 0.7, while no maximum occurs for x=0.8. This strongly suggests the disappearance of AFM in these orthorhombic phases, which would be a consequence of the reduction of the number of antiferromagnetic superexchange interactions. A ferromagnetic ordered state still develops, as indicated the presence of irreversibility that actually starts above room temperature for x=0.6, and above the measuring range for x=0.7 and 0.8 (and likely 0.9). Note the existence of distinctive ferromagnetic hysteresis loops at 5 K

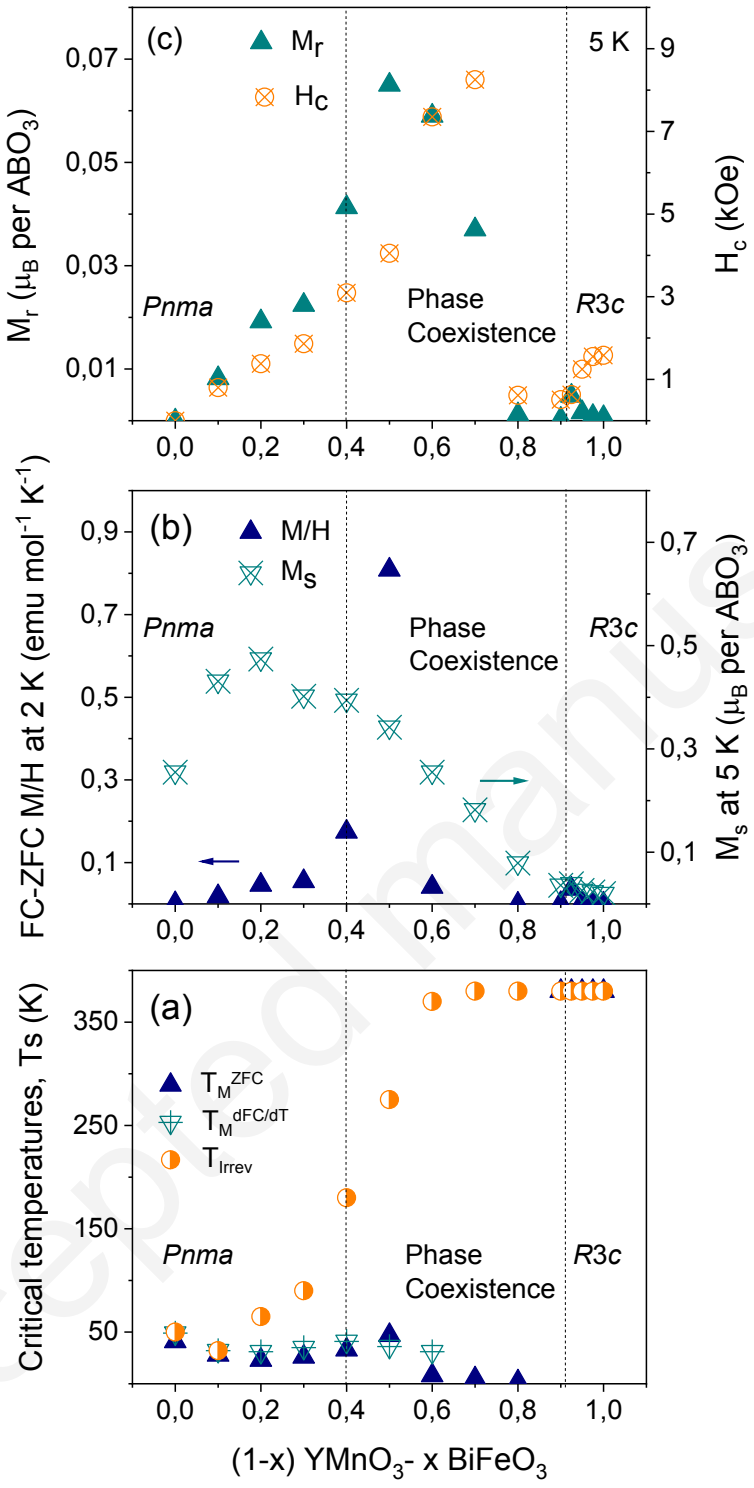

Fig. 6. Compositional dependence of magnetic parameters; (a) critical temperatures in ZFC/FC curves (T_M^{ZFC}: maximum *M/H* in ZFC; $T_M^{dFC/dT}$: maximum derivative in FC; T_{Irrev}: splitting of the ZFC and FC curves), (b) Difference between FC and ZFC magnetizations at 2 K and magnetization at 5 K and 50 kOe, and (c) remnant magnetization and coercive field at 5 K.

for x=0.6 and 0.7 (see Fig. 4(b)). Loop parameters as a function of composition are given in Fig. 6(c). Remnant magnetization continuously increases across the orthorhombic phase up to 0.065μ_B per ABO_3 for x=0.5, above which it decreases. Coercive field keeps increasing until x=0.7 up to a value of 8.25 kOe. Residual competing antiferromagnetic interactions exist, and are most probably responsible for the low temperature maxima in the ZFC curve for x=0.6 an 0.7 that would then be associated with spin glass behavior. Composition x=0.8 is already a transition one with magnetic response partially controlled by the rhombohedral phase.

Although general behavior across the orthorhombic field can be roughly understood from a competition between the decreasing antiferromagnetic superexchange Mn^{3+}-O^{2-}-Mn^{3+} interactions, and increasing ferromagnetic double exchange Mn^{3+}-O^{2-}-Fe^{3+} ones, the possible presence of Mn^{4+} and/or Fe^{2+} and thus, of additional magnetic interactions, must be also considered. Actually Mn^{4+} has been reckoned necessary to stabilize the metastable perovskite phase at ambient pressure [39]. A Curie-Weiss analysis was carried out for all orthorhombic phases up to x=0.4, and results are shown in Fig. 7. In the case of $YMnO_3$, an effective paramagnetic moment of 4.93μ_B was obtained, which suggests the absence or very low concentration of Mn^{4+} (spin-only magnetic moment of Mn^{3+} is 4.90μ_B). Situation changes after the substitution of Bi^{3+}/Fe^{3+} for Y^{3+}/Mn^{3+}, and increasing deviations of the obtained effective paramagnetic moments from expected ones (according to the spin-only magnetic moments of Mn^{3+} and Fe^{3+}: 4.90 and 5.92μ_B, respectively) are found. An experimental value of 4.60 μ_B is obtained for x=0.1 (5.0 μ_B anticipated). This would indicate a Mn^{4+} fraction of 0.43 that seems too high, for A or B-site vacancies must occur at the same time. Alternatively, one can assume the simultaneous presence of Fe^{2+} (along with oxygen vacancies), that would reduce the Mn^{4+} fraction down to 0.32 for this composition in the unlikely limit case (all Fe^{3+} reduced to Fe^{2+}). Similar arguments apply to all compositions up to x=0.4. Even though obtained effective moments slightly depend on the high temperature interval considered for

the C-W fit, and so do Mn^{4+} fractions, its presence along with Fe^{2+} is clearly indicated. This was confirmed by XPS (see Supplementary information).

Rhombohedral phases are present from x=0.5 up to x=1, as majority polymorphic form for x=0.9, and as single phase from x=0.925 up to x=1. Two compositional intervals can be distinguished across the rhombohedral solid solution regarding its magnetic response, and specifically the magnetization values. These would be from x=0.9 (and most probably from below, for AFM characteristics are present in x=0.7 and 0.8, even though properties of the minor rhombohedral phases cannot be isolated) up to 0.95, and from x=0.975 up to x=1. All phases, at least from x=0.9 ad up to x=1, are antiferromagnetic with a Neel temperature that is above the measuring range, and that increases with x according to DTA results [27]. Main difference is magnetization, and the temperature at which irreversibility starts that seem both higher in the first interval. This might be associated with the spin cycloid characteristic of $BiFeO_3$, which would be absent for x≤0.95.

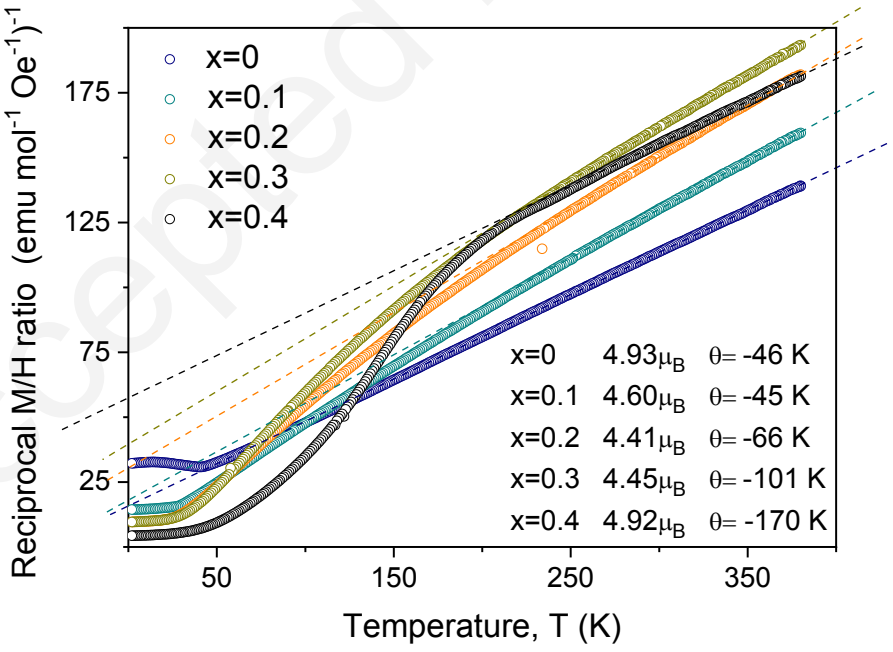

Fig. 7. Curie-Weiss analysis of the static susceptibility for the orthorhombic single-phase (1-x) $YMnO_3$-x $BiFeO_3$ materials.

Nonetheless, the possible presence of magnetic impurities below the sensitivity of XRD must be considered, for this is a recurrent issue when $BiFeO_3$ based materials are addressed [11]. This was studied for x=0.925, which showed the highest magnetization and irreversibility levels (see Fig. 5). A new set of samples thermally treated at increasing temperatures from 650 up to 900 ºC were characterized. This experiment was devised to reveal any possible secondary phase going unnoticed in the sample thermally treated at 825 ºC. However, no unreacted oxides or intermediate phases were revealed in samples treated at 650 or 700 ºC, nor decomposition products were found for that treated at 900 ºC. XRD patterns for all materials are given in the supplementary information. Only noticeable effect was the peak width that clearly decreased as temperature was increased. This is most probably an effect of crystal size, because particle size increases from 65-80 nm for the materials thermally treated at 650 and 700 ºC, up to 0.5 μm and above the micron for those annealed at 825 and 900 ºC, respectively. Note that peak splitting associated with the rhombohedral distortion is only resolved for the two latter cases. This increase in crystal size has significant effects on the magnetic properties, as shown in Fig. 8. Indeed, a distinctive increase of magnetization takes place when the temperature of the thermal treatment is raised from 700 up to 825 ºC, i.e. when particle size is increased out of the nanoscale. *M/H* ratio at 380 K is only 0.0065 emu mol^{-1} Oe^{-1} for the sample treated at 700 ºC, and 0.0636 emu mol^{-1} Oe^{-1} for that treated at 825 ºC, further raised up to 0.3181 emu mol^{-1} Oe^{-1} after the treatment at 900 ºC. Irreversibility also shows a similar increase with size, and a FC ratio of 0.346 emu mol^{-1} Oe^{-1} is reached at 2 K for the latter sample. This is accompanied by a distinctive enhancement of the new ferromagnetic contribution in the high field magnetization at 5 K, with M_r and H_c values of $\approx 0.0028\mu_B$ and 55 Oe, respectively.

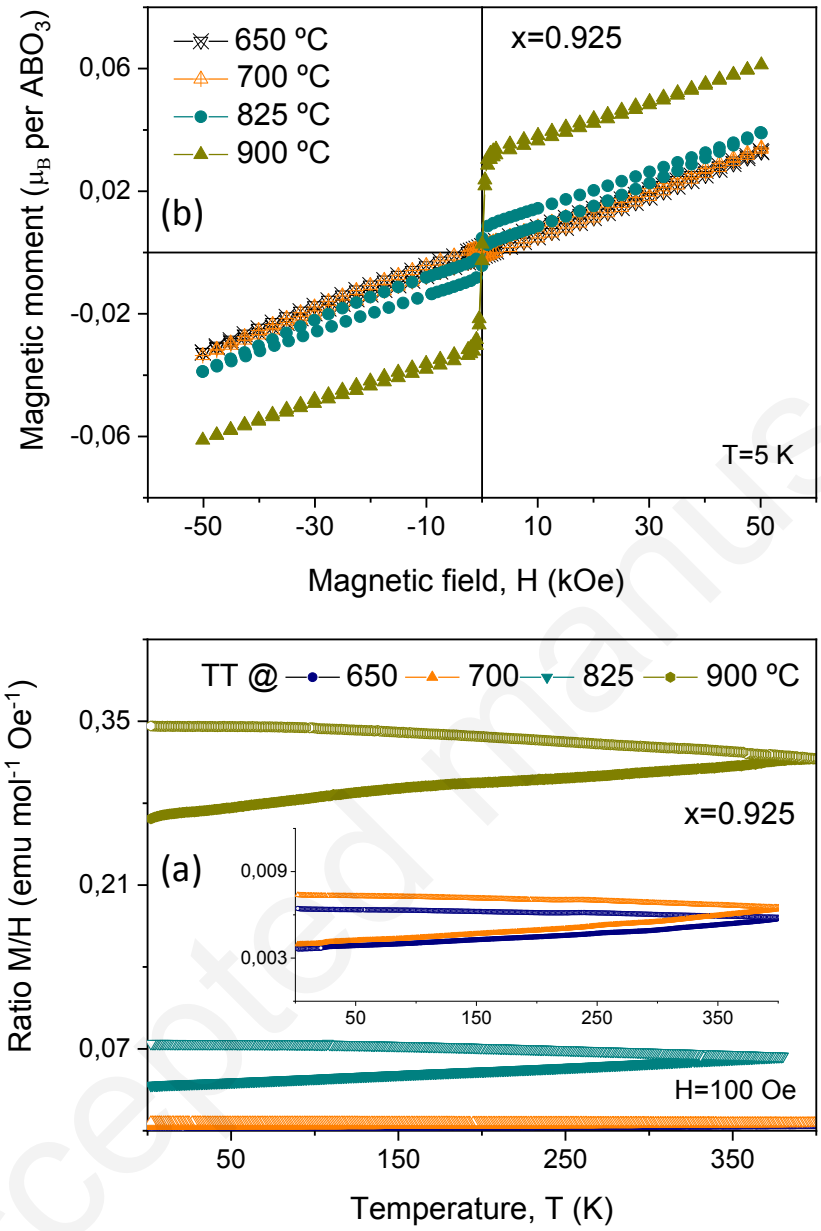

Fig. 8. (a) Temperature dependence of the ZFC (close symbols) and FC (open symbols) static susceptibility, and (b) isothermal magnetization at 5 K for rhombohedral single-phase (1-x) $YMnO_3$-x $BiFeO_3$ materials with x=0.925, after thermal treatments at increasing temperature.

These results seem to rule out a role of magnetic impurities, and to uncover instead an effect of crystal size on spin canting and the associated weak ferromagnetism for rhombohedral phases. This spin canting would only take place for phases with x between x=0.9 and 0.95. Note that the perovskite oxide with x=0.9 could not be treated above 750 ºC before decomposing, so crystal sizes beyond the nanoscale were not attained in this case. Note also that spin canting is not observed for x=0.975, in spite of this composition having been thermally treated at 825 ºC. This suggests the cycloidal modulation of the G-type antiferromagnetic arrangement to be absent for phases up to x=0.95, and present for x=0.975.

Magnetic characterizations have revealed polymorphic phases in coexistence across the system to have differentiated properties. Most interesting interval might be from x=0.6 up to 0.9, for which coexistence between nonpolar orthorhombic ferromagnetic phases and polar rhombohedral antiferromagnetic ones, the latter then multiferroic, seem to occur at room temperature. Equal phase percentages must be obtained for a composition between x=0.8 and 0.9, and strong magnetoelectric responses can be expected from their interaction whether it is elastic, electrostatic or magnetic [47]. However, studying coupling requires solving ceramic processing, challenging because phases in this range decompose when heated above 550-750 ºC. Electrical poling of ceramics is also necessary, which might be not straightforward either. Hopping conductivity is often an issue in multiferroic oxides when different species and valence states are present at the B-site, as it is the case here. A specific study addressing both issues has recently been reported [48].

5. Conclusions

Two stable and continuous perovskite solid solutions with orthorhombic *Pnma* and rhombohedral *R*3*c* symmetries are present in the (1-x) $YMnO_3$-x $BiFeO_3$ binary system, which coexist across a

wide compositional range that spans from x=0.5 up to 0.9, with varying percentages. The two perovskite polymorphic forms show distinctive magnetic properties with differentiated evolutions within each solid solution. For orthorhombic phases with x-values ranging from x=0 up to 0.9, three compositional regions can be distinguished regarding their magnetic response. The antiferromagnetic ordering of $YMnO_3$ seems to be basically preserved up to x=0.1, though a decrease of the Neel temperature and the appearance of irreversibility, indicating spin canting, are found. For x=0.2 up to 0.5, a canted antiferromagnet still exists, but the ferromagnetic component is gradually enhanced, at the same time ordering develops at increasingly high temperatures. From x=0.6, antiferromagnetic features were not observed anymore, though the ferromagnetic behaviour remains, and is already observed at room temperature. Relating rhombohedral phases present from x=0.5 up to x=1, and as majority or single-phase from $x \geq 0.9$, antiferromagnetic ordering is indicated for all compositions with Neel temperatures above 380 K. Spin canting and weak ferromagnetism that is enhanced by particle coarsening are observed for x-values between 0.9 and 0.95, but not for x=0.975 and x=1. Two compositional intervals exist then in the rhombohedral region, most probably associated with the destruction of the long range cycloidal modulation of $BiFeO_3$ as x decreases. Overall, these results define a compositional region between x=0.6 and 0.9, where a non-polar orthorhombic ferromagnetic perovskite phase coexist at room temperature with a polar rhombohedral canted antiferromagnet. Large phase-change magnetoelectric responses can then be expected, associated with the electrically induced phase transformation between the two polymorphic phases.

Acknowledgements. Research funded by Spanish MICINN through project MAT2017-88788-R. J.A. Quintana-Cilleruelo also recognizes additional funding by Spanish MINECO (grant BES-2015-072595), and training in JANA2006 during a two-month research stay at Ecole Centrale Paris under

the supervision of Dr. Brahim Dkhil. Technical support by Ms. I. Martínez at ICMM-CSIC, and magnetic data acquisition by Mr. T. Guizouarn at ISCR are greatly acknowledged.

References

[1] N.A. Spaldin, M. Fiebig, The renaissance of magnetoelectric multiferroics, Science 309 (2005) 391-392.

[2] W. Eerenstein, N.D.Mathur, J.F. Scott, Multiferroic and magnetoelectric materials, Nature 442 (2006) 759-765.

[3] T. Zhao, A. Scholl, F. Zavaliche, K. Lee, M. Barry, A. Doran, M.P. Cruz, Y.H. Chu, C. Ederer, N.A. Spaldin, R.R. Das, D.M. Kim, S.H. Baek, C.B. Eom, R. Ramesh, Electrical control of antiferromagnetic domains in multiferroic $BiFeO_3$ films at room temperature, Nature Mat. 5 (2006) 823-829.

[4] N.A. Spaldin, R. Ramesh, Advances in magnetoelectric multiferroics, Nature Mat. 18 (2019) 203-212.

[5]. M. Bibes, A. Barthelemy, Multiferroics: Towards a magnetoelectric memory, Nature Mat. 7 (2009) 425-426.

[6] S. Fusil, V. Garcia, A. Barthelemy, M. Bibes, Magnetoelectric devices for spintronics, Ann. Rev. Mater. Res. 4 (2014) 91-116.

[7] G. Dong, Z. Zhou, X. Zue, Y. Zhang, B. Peng, M. Guan, S. Zhao, Z. Hu, W. Ren, Z.G. Ye, Ferroelectric phase transition induced a large FMR tuning in self-assembled $BaTiO_3$:$Y_3Fe_5O_{12}$ multiferroic composites, ACS Appl. Mater. Interfaces 9 (2017) 30733-30740.

[8] D. Khomskii, Classifying multiferroics: Mechanisms and effects, Physics 2 (2006) 20.

[9] R. Seshadri, N.A. Spaldin, Visualizing the role of Bi 6s "lone pairs" in the off-center distortion in ferromagnetic $BiMnO_3$, Chem. Mater. 13 **(**2001) 2892-2899.

[10] J. Wang, J.B. Neaton, H. Zheng, V. Nagarajan, s.B. Ogale, B. Liu, D. Viehland, V. Vaithyanathan, D.G. Schlom, U.V. Waghmare, N.A. Spaldin, K.M. Rabe, M. Wuttig, R. Ramesh, Epitaxial $BiFeO_3$ multiferroic thin film heterostructures, Science 299 (2003) 1719-1722.

[11]. G. Catalan, J.F. Scott, Physics and applications of bismuth ferrite, Adv. Mater. 21 (2009) 2463-2485.

[12] J.M. Moreau, C. Michel, R. Gerson, W.J. James, Ferroelectric $BiFeO_3$ X-ray and neutron diffraction study, J. Phys. Chem. Solids 32 (1971) 1315-1320.

[13] I. Sosnowska, T. Peterlin-Neumaier, E. Steichele, Spiral magnetic ordering in bismuth ferrite, J. Phys. C: Solid State Phys. 15 (1982) 4835–4846.

[14] T.J. Park, G.C. Papaefthymiou, A.J. Viescas, A.R. Moodenbaugh, S.S. Wong, Size-dependent magnetic properties of single-crystalline mutiferroic $BiFO_3$, Nano Lett. 7 (2007) 766-772.

[15] V.A. Khomchenko, D.A. Kiselev, J.M. Vieira, L. Jian, A.L. Kholkin, A.M.L. Lopes, Y.G. Pogorelov, J.P. Araujo, M. Maglione, Effect of diamagnetic Ca, Sr, Pb and Ba substitution on the crystal structure and multiferroic properties of the $BiFeO_3$ perovskite, J. Appl. Phys. 103 (2008) 024105.

[16] F.M. Bai, J.L. Wang, M. Wuttig, J.F. Li, N.G. Wang, A.P. Pyatakov, A.K. Zvezdin, L.E. Cross, D. Viehland, Destruction of spin cycloid in $(111)_c$-oriented $BiFeO_3$ thin films by epitaxial constraint: Enhanced polarization and release of latent magnetization, Appl. Phys. Lett. 86 (2005) 032511.

[17] J.T. Heron, J.L. Bosse, Q. He, Y. Gao, M. Trassin, L. Ye, J.D. Clarkson, C. Wang, J. Liu, S. Salahuddin, D.C. Ralph, D.G. Schlom, J. Iñiguez, B.D. Huey, R. Ramesh, Deterministic switching of ferromagnetism at room temperature using an electric field, Nature 516 (2014) 370-375.

[18] S.W. Cheong, M. Mostovoy, Multiferroics: a magnetic twist for ferroelectricity, Nature Mat. 6 (2007) 13-20.

[19]. T. Kimura, T. Goto, H. Shintani, K. Ishizaka, T. Arima, Y. Tokura, Magnetic control of ferroelectric polarization, Nature 426 (2003) 55-58.

[20] B. Dabrowski, S. Kolesnik, A. Baszczuk, O Chmaissem, T. Maxwell, J. Mais, Structural, transport, and magnetic properties of $RMnO_3$ perovskites (R = La, Pr, Nd, Sm, Eu-153, Dy), J. Solid State Chem. 178 (2005) 629-637.

[21] J.S. Zhou, J.B. Goodenough, J.M. Gallardo-Amores, E. Morán, M.A. Alario-Franco, R. Caudillo, Hexagonal versus perovskite phase of manganite $RMnO_3$ (R=Y, Ho, Er, Tm, Yb, Lu), Phys. Rev. B 74 (2006) 014422.

[22] H.L. Yakel, W.C. Koehler, E.F. Bertaut, E.F. Forrat, On the crystal structure of the manganese (III) trioxides of the heavy lanthanides and yttrium, Acta Cryst. 16 (1963) 957-962.

[23] A. Muñoz, J.A. Alonso, M.J. Martínez-Lope, M.T. Casais, J.L. Martinez, M.T. Fernandez-Diaz, Magnetic structure of hexagonal $RMnO_3$ (R=Y, Sc): Thermal evolution from neutron diffraction data, Phys. Rev. B 62 (2000) 8498-9510.

[24] B.B. Van Aken, T.T.M. Palstra, A. Filippetti, N.A. Spaldin, The origin of ferroelectrcitiy in magnetoelectric $YMnO_3$, Nature Mat. 3 (2004) 164-170.

[25] A.S. Gibbs, K.S. Knight, P. Lightfoot, High-temperature phase transitions in hexagonal $YMnO_3$, Phys. Rev. B 82 (2011) 094111.

[26] A. Moure, T. Hungría, A. Castro, J.Galy, O. Peña, J. Tartaj, C. Moure, Doping influence on the stability of $YMnO_3$ orthorhombic pervoskite obtianed by mechanosynthesis, Mater. Chem. Phys. 133 (2012) 764-771.

[27] J.A. Quintana-Cilleruelo, V.K. Veerapandiyan, M. Deluca, M. Algueró, A. Castro, Mechanosynthesis of the whole $Y_{1-x}Bi_xMn_{1-x}Fe_xO_3$ perovskite system: Structural characterization and study of pahse transitions, Materials 12 (2019) 1515.

[28] I. Fina, L. Fábrega, X. Martí, F. Sánchez, J. Fontcuberta, Magnetic switch of polarization in epitaxial orthorhombic $YMnO_3$ thin films, Appl. Phys. Lett. 97 (2010) 232905.

[29] B. Lorenz, Y.Q. Wang, Y.Y. Sun, C.W. Chu, Large magnetodielectric effects in orthorhombic $HoMnO_3$ and $YMnO_3$, Phys. Rev. B 70 (2004) 212412.

[30] B. Lorenz, Y.Q. Wang, C.W. Chu, "Ferroelectricity in perovskite $HoMnO_3$ and $YMnO_3$, Phys. Rev. B 76 (2007) 104405.

[31] D. Kan, L. Pálová, V. Anbusathaiah, C.J. Cheng, S. Fujino, V. Nagarajan, K. Rabe, I. Takeuchi, Universal behavior and electric-field-Induced structural transition in rare-earth-substituted $BiFeO_3$, Adv. Funct. Mater. 20 (2010) 1108–1115.

[32] B. Xu, D. Wang, J. Iñiguez, L. Bellaiche, Finite-temperature properties of rare-earth-substituted $BiFeO_3$ multiferroic solid solutions, Adv. Funct. Mater. 25 (2014) 552-558.

[33] D. Damjanovic, A morphotropic phase boundary system based on polarization rotation and polarization extension, Appl. Phys. Lett. 97 (2010) 062906.

[34] C.M. Fernández-Posada, A. Castro, J.M. Kiat, F. Porcher, O. Peña, R. Jiménez, M. Algueró, H. Amorín, The polar/antipolar phase boundary of $BiMnO_3$ -$BiFeO_3$ -$PbTiO_3$: Interplay among crystal structure, point defects, and multiferroism, Adv. Funct. Mater. 28 (2018) 1802338.

[35] S.N. Triphathy, K.K. Mishra, S. Sen, B.G. Mishra, D.K. Pradhan, R. Palai, D.K. Pradhan, Phase transition and magneto-electric coupling of $BiFeO_3$-$YMnO_3$ multiferroic nanaoceramics, J. Appl. Phys. 114 (2013) 144104.

[36] R. Pandey, L.K. Pradhan, P. Kumar, M Kar, Double crystal symmetries and magnetic orderings in co-substituted (Y and Mn) bismuth ferrite, Ceram Int. 44 (2018) 18609–18616.

[37] A.V. Nazarenko, A.G. Razumnaya, M.F. Kupriyanov, Y.V. Kabirov, A.G. Rudskaya, P.Y. Teslenko, N.B. Kofanova, Specific features of structural states in the $BiFeO_3$-$YMnO_3$ solid solutions, Phys. Solid State 53 (2011) 1599-1602.

[38] V. Petrícek, M. Dušek, L. Palatinus, Crystallographic computing system JANA2006: General features, Zeitschrift fur Krist. 229 (2014) 345–352.

[39] A. Muñoz, J.A. Alonso, M.T. Casais, M.J. Martínez-Lope, J.L. Martínez, M.T. Fernández-Díaz, The magnetic structure of $YMnO_3$ perovskite revisited, J. Phys.: Condens. Matter 14 (2002) 3285-3294.

[40] W.M. Zhu, H.Y. Guo, Z.G. Ye, Structural and magnetic characterization of multiferroic $(BiFeO_3)_{1-x}(PbTiO_3)_x$ solid solutions, Phys. Rev. B 78 (2008) 014401.

[41] M.K. Singh, W. Prellier, M.P. Singh, R.S. Katiyar, J.F. Scott, Spin-glass transition in single-crystal $BiFeO_3$, Phys. Rev. B 77 (2008) 144403.

[42] C.M. Fernández-Posada, H. Amorín, C. Correas, O. Peña, M. Algueró, A. Castro, Mechanosynthesis and multiferroic properties of the $BiFeO_3$-$BiMnO_3$-$PbTiO_3$ ternary system along its morphotropic phase boundary, J. Mater. Chem. C 3 (2015) 2255-2265.

[43] B. Noheda, J.A. Gonzalo, L.E. Cross, R. Guo, S.E. Park, D.E. Cox, G Shirane, Tetragonal-to-monoclinic phase transition in a ferroelectric perovskite: The structure of $PbZr_{0.52}Ti_{0.48}O_3$, Phys. Rev. B 61 (2000) 8687.

[44] J. Chaigneau, J. M. Kiat, C. Malibert, C. Bogicevic, Morphotropic phase boundaries in $(BiScO_3)_{1-x}(PbTiO_3)_x$ ($0.6<x<0.75$) and their relation to chemical composition and polar order, Phys. Rev. B 76 (2007) 094111.

[45] W. Jo, J.E. Daniels, J.L. Jones, X. Tan, P.A. Thomas, D. Damjanovic, J. Rodel, Evolving morphotropic phase boundary in lead-free $(Bi_{1/2}Na_{1/2})TiO_3$-$BaTiO_3$ piezoceramics J. Appl. Phys. 109 (2011) 014110.

[46] O. Diéguez, J. Iñiguez, First-principles investigation of morphotropic transitions and phase-change functional responses in $BiFeO_3$-$BiCoO_3$ multiferroic solid solutions, Phys. Rev. Lett. 107 (2011) 1–5.

[47] J.M. Hu, L.Q. Chen, C.W. Nan, Multiferroic heterostructures integrating ferroelectric and magnetic materials, Adv.Mater. 28 (2016) 15-39.

[48] J.A. Quintana-Cilleruelo, A. Castro, H. Amorín, V.K. Veerapandiyan, M. Deluca, O. Peña, M. Algueró, Ceramic processing and multiferroic properties of the perovskite $YMnO_3$ – $BiFeO_3$ binary system. J. Am. Ceram. Soc. 103 (2020) 4846-4858

Supplementary data

Supplementary Rietveld analysis

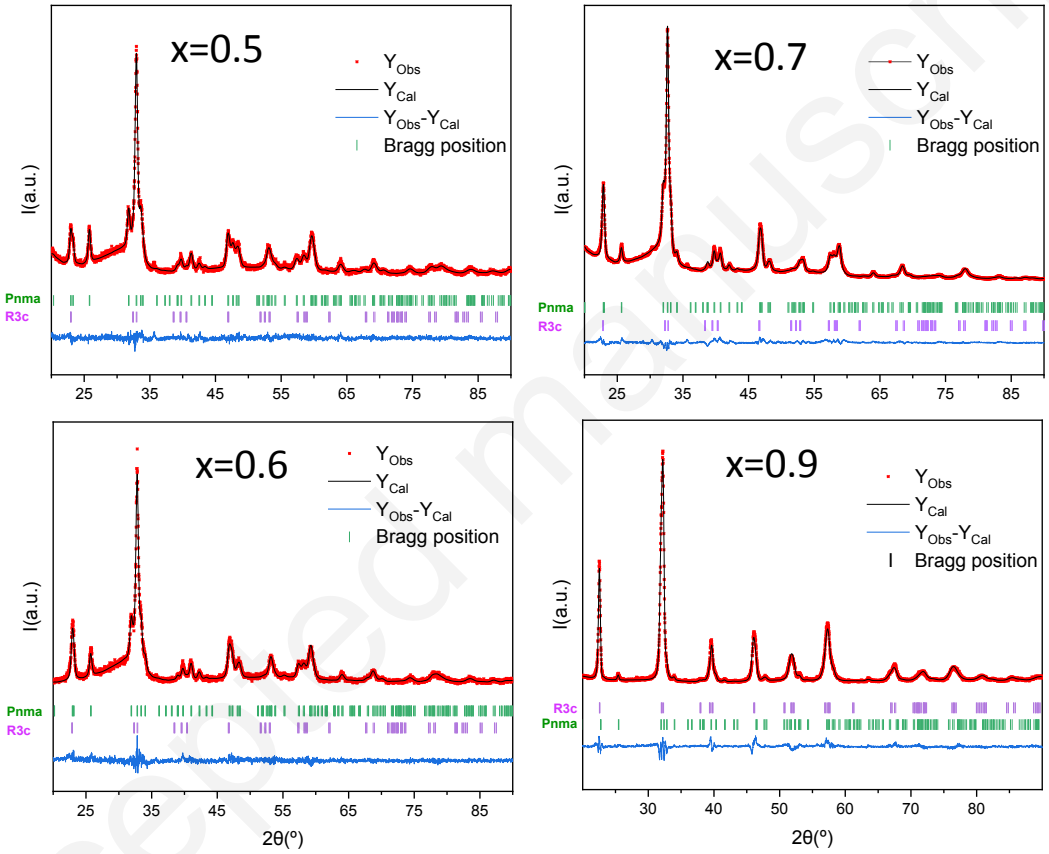

Figure S1. Rietveld analysis of XRD data for the rest of the (1-x) $YMnO_3$-x $BiFeO_3$ materials in the phase coexistence region, assuming a mixed orthorhombic *Pnma* and rhombohedral *R3c* model. Note the evolution from a majority orthorhombic phase to a majority rhombohedral one as x increases. Refined orthorhombic fractions are provided in the article (Table 1).

Supplementary XPS data

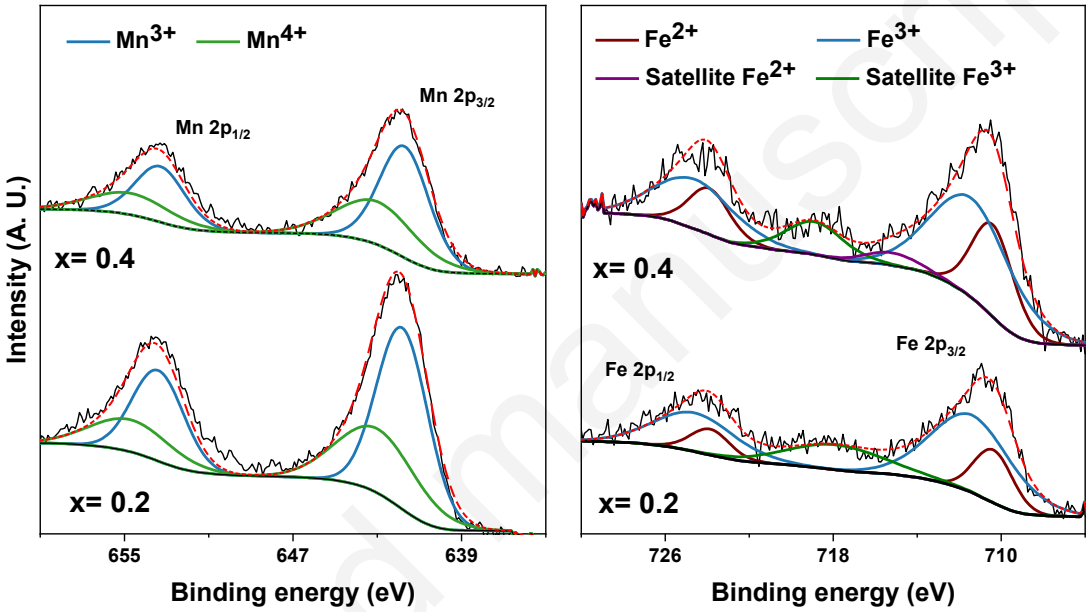

Figure S2. XPS spectra for the (1-x) $YMnO_3$-x $BiFeO_3$ materials with x=0.2 and 0.4 (orthorhombic región) in the energy intervals across the Mn 2p and Fe 2p lines. Note the presence of Mn^{4+} and Fe^{2+} contributions, along with the Mn^{3+} and Fe^{3+} ones for both the $2p_{1/2}$ and $2p_{3/2}$ signals. Satellite Fe 2p lines are also indicated. A SPEC GmbH spectrometer with UHV system, equipped with a PHOIBOS 150 9 MCD energy analyzer (SPECS Surface Nano Analysis GmbH, Berlin, Germany), and an Al (1486.74 eV) monochromatic source with a power of 200 W and a voltage of 12 kV were used to carry out the analysis.

Supplementary XRD data

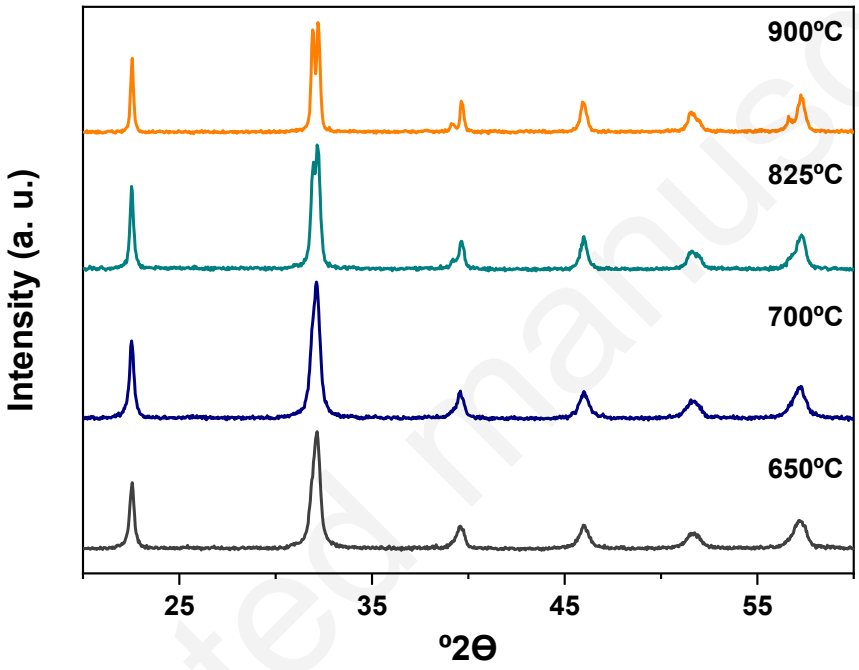

Fig. S3. XRD patterns for (1-x) $YMnO_3$-x $BiFeO_3$ materials with x=0.95 (rhombohedral region), thermally treated at increasing temperatures. Note the absence of secondary phases for all cases, and the increased crystallinity as temperature is raised, so that the rhombohedral distortion is resolved after heating at 825 ºC.